CCFE
CULHAM CENTRE FOR FUSION ENERGY

UK Atomic Energy Authority

UKAEA-CCFE-PR(22)25

Mia Maric, Rhys Thomas, Tamas Ungar, Gyula Zilahi, Callum Hunt, David Lunt, Jack Donoghue, Kieran Lynch, Philipp Frankel, Pierre Barberis, Florent Bourlier, Michael Preuss, Pratheek Shanthraj

CHARACTERISATION OF HYDRIDE PRECIPITATION AND REORIENTATION IN ZIRCONIUM ALLOYS AT DIFFERENT METALLURGICAL STATES

CHARACTERISATION OF HYDRIDE PRECIPITATION AND REORIENTATION IN ZIRCONIUM ALLOYS AT DIFFERENT METALLURGICAL STATES

Mia Maric, Rhys Thomas, Tamas Ungar, Gyula Zilahi, Callum Hunt, David Lunt, Jack Donoghue, Kieran Lynch, Philipp Frankel, Pierre Barberis, Florent Bourlier, Michael Preuss, Pratheek Shanthraj

This is a preprint of a paper submitted for publication in
ASTM Zirconium in the Nuclear industry conference proceedings

CHARACTERISATION OF HYDRIDE PRECIPITATION AND REORIENTATION IN ZIRCONIUM ALLOYS AT DIFFERENT METALLURGICAL STATES

Mia Maric[1], Rhys Thomas[1], Tamas Ungar[1], Gyula Zilahi[2], Callum Hunt[1], David Lunt[1], Jack Donoghue, Kieran Lynch[1], Philipp Frankel[1], Pierre Barberis[3], Florent Bourlier[4], Michael Preuss[1,5], Pratheek Shanthraj[1]

[1] *Department of Materials, The University of Manchester, Manchester M13 9PL, U*

[2]*UK Atomic Energy Authority, Culham Science Centre, Abingdon, Oxon, OX14 3DB, UK*

[3] *Framatome, CRC, Avenue Paul Girod, CS 90100, 73403 Ugine Cedex, France*

[4] *Framatome, 12 rue Juliette récamier, 69006 Lyon Cedex, France*

[5]*Department of Materials Science and Engineering, Monash University, Clayton, 3800, Australia*

ABSTRACT

Hydride precipitation and reorientation has the potential to embrittle zirconium alloys. This study aims to better understand the influence of the Zr microstructure on hydride precipitation and reorientation. Specifically, the crystallography, phase stability and morphology of hydride precipitation was correlated to microstructural variations due to changes in the metallurgical state of the zirconium alloy. The work highlights, that microstructural features induced during recrystallisation have a significant influence on the distribution and orientation of hydrides when no external stress is applied. The stability of γ hydride was shown to be dictated by metallurgical state whereby its formation was promoted in the recrystallised sample owing to its reduced strength. The influence of grain orientation on γ stability was also explored. It was highlighted that upon cooling, grains oriented in the $<10\bar{1}0>$ direction are under compression such that γ hydride formation is supressed. This study showed that the metallurgical state did not have a significant influence on the extent of hydride reorientation during thermomechanical loading, but rather extrinsic factors such as the applied stress and temperature dictated reorientation behaviour. Quantification of the dislocation density in both the matrix and hydride during precipitation highlighted that extensive matrix recovery takes place during hydriding. It was also shown that the dislocation density in the hydride is lower after thermomechanical loading whereby the application of both a hoop and axial stress during reprecipitation enabled greater accommodation of the volumetric expansion that occurs during precipitation.

1. INTRODUCTION

Hydride precipitation during both in-service operations and dry storage of zirconium (Zr) cladding tubes can result in embrittlement and potential crack-induced failure[292–298]. Due to this, a number of studies have characterised the hydrides produced under operational and end of life storage conditions[8,89,129,132,145,167]. In both situations, it has been shown that hydrides adopt a platelet like shape when precipitating parallel to the basal plane of the Zr matrix. This is due to strain induced during hydride precipitation in Zr stemming from the volumetric mismatch between the two phases[6]. Further, it has been shown that the mesoscale hydrides consist of nano scale packets of hydride platelets that stack together to reduce the strain energy around the hydrides[6,37,237,238].

Importantly, when going from in-service operation to dry storage conditions the arrangement of the hydride platelets might change. In conditions without the application of an external load, the texture, grain size and morphology due to pilgering results in the precipitation of hydrides platelets along the circumferential direction[6,8,9,146,167]. However, during dry storage, cladding tubes are subject to a series of sequential drying stages. Here, the increased temperature of the cladding together with the fission gas produced during operation results in hydride dissolution and the generation of a tensile hoop stresses on the cladding[144]. In addition, the lifting of the fuel assemblies during handling with the fuel pellets still inside can also result in significant axial stresses. During cooling, if the stress exerted exceeds a critical level, reorientation of the hydrides will occur. The alignment of hydrides in the radial direction forms brittle paths along which radial cracks can form and propagate – causing catastrophic cladding failure [6,244].

The critical axial stress required to cause reorientation is a debated topic within literature, with reported values ranging from 70-200MPa[10,145,154–156,158]. The large variation could be due to a myriad of factors, such as differences in hydrogen concentration, metallurgical state, thermo-mechanical process history and multiaxial stress state of the material [6,10,299]. Studies by Cinbiz et al.[10] have highlighted that increasing biaxiality ratios of the applied stress causes the critical stress for reorientation to reduce by up to 50% highlighting the importance of identifying and characterising multiaxial stress levels. Importantly, no dedicated study correlating the metallurgical state to critical reorientation stress has been conducted to date. However comparing separate studies on cold-work stress relieved[8,150,159,232] and recrystallised[10] materials suggest that the critical stress might be within the same range for both metallurgical states. This could indicate that the onset of hydride reorientation is not heavily controlled by microstructural features but rather extrinsic factors such as the stress state of the material.

On the other hand, it is believed that the matrix microstructure can have an influence on the distribution, morphology and microstructure of the precipitating hydride. Colas et al[119], as well as Nagase et al[155], have suggested that the difference in grain size and shape between the stress-relieved and recrystallised microstructures can have an influence on the orientation and length of the hydrides produced during precipitation. Here, it was suggested that shorter intergranular hydrides with a greater radial hydride component would be found in a recrystallised rather than cold-worked matrix microstructure. This could be due to the greater radial grain boundary component in the equiaxed grains as well as their smaller size when compared to the elongated cold-worked grains. However, no evidence for these hypotheses has been provided and the influence of other features such as dislocations and crystallographic texture on the extent of hydride precipitation and reorientation has not yet been explored.

Therefore, the principal aim of this study was to correlate microstructural features induced during both deformation and recrystallisation to the precipitation and reorientation of hydrides

upon cooling. Here, electron backscatter diffraction in conjunction with back-scatter electron imaging and x-ray diffraction was utilised to characterise the microstructure and defects before hydriding as well as after hydride precipitation and reorientation respectively such that correlations between the two could be made. Importantly, three different reorientation stresses with varying biaxiality ratios were selected for the reorientation experiments such that any correlations between stress and metallurgical state could be made.

2. METHODS

2.1 SAMPLE INFORMATION

The samples in this study were provided by Framatome and are cold-work stress relieved Zircaloy-4 cladding tubes that have undergone standard pilgering and stress relieving protocols, which is a heat treatment at 485 °C. The stress relieving procedure was performed within the temperature range of 470-490 ^{o}C for several hours. After this, 10 cm long segments of the cladding were heated to 520, 560 and 730 °C in a vacuum furnace followed by furnace cooling. The holding times at 520 and 560 °C was 1 hour and to encourage extensive grain growth the hold time for the heat treatment at 730 °C was 3 hours. Therefore, in this study, samples at four different metallurgical states were studied: stress relieved (485 ^{o}C), partially recrystallised (520 °C), recrystallised (560 °C) and recrystallised with substantial grain growth (730 °C).

2.2 HYDRIDING PROCEDURE

The samples were subsequently gas-hydrided to a hydrogen content ranging from 200-300 ppm. Here, the samples were held at 400 ^{o}C in a hydrogen rich atmosphere and constant pressure. Initially, samples were all heated to consistent times. However, it was apparent that the recrystallised sample had a significantly lower hydrogen concentration when compared to the deformed sample. Therefore, the hold times were adjusted for each metallurgical state to obtain similar hydrogen content. The respective hydrogen concentrations for each sample are also shown in Table 2.1. At the end of the gas-charging procedure, samples were furnace cooled at a rate of 1 ^{o}C/min. Despite the best efforts, it is apparent that the hydrogen content for the stress-relieved sample is around 100 ppm lower than for the other three samples.

Table 2.1 Hydriding time for samples at different metallurgical states

Pre-Hydriding Metallurgical State	Temperature (°C)	Time (h)	Hydrogen Content (ppm)
Stress Relieved	485	3.75	201
Partially Recrystallised	520	10	339
Recrystallised	560	10	290
Recrystallised + Grain Growth	730	10	357

2.3 HYDRIDE REORIENTATION PROCEDURE

After hydriding, the samples were subject to reorientation testing using an in-house rig developed by Framatome, as shown in Figure 2.1a. Here, the sample was heated to a temperature of 400 ^{o}C in the radiative furnace. Additionally, the internal pressure-controlled

system coupled with a CAT.1 Creep Advanced Testing Machine enabled the application of both an axial and hoop stress to the sample such that the stress biaxiality can be varied. At the end of the thermomechanical cycle, the sample was furnace cooled at a rate of 1 °C/min. An example of a temperature and stress profiles is shown in Figure 2.1b. In this study, three different stress combinations were utilised such that the influence on stress biaxiality could be determined, see Table 2.2.

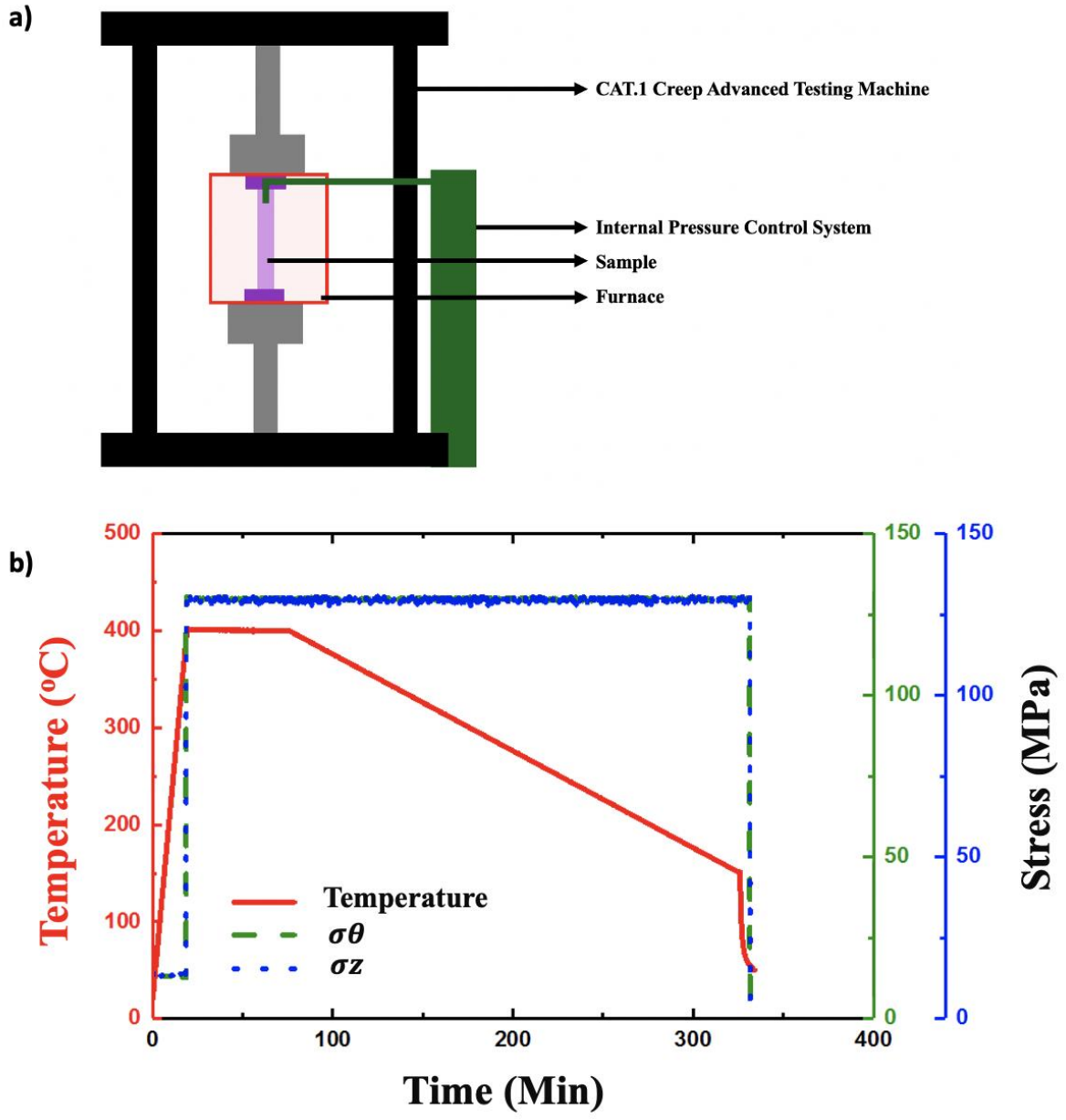

Figure 2.1 a) In house developed reorientation rig consisting of an internal pressure control system as well as tensile rig such that biaxial stresses (i.e., axial and hoop stresses) can be applied to the cladding. A radiative furnace is shown by the red box which is responsible for heating the sample, during the testing axial and hoops strains are measured by laser extensometers. b) Temperature and stress curves during the reorientation experiment. This is an example of the stress curve at 130MPa.

Table 2.2 Axial and Hoop stresses utilised for reorientation testing

Axial Stress (σ_z)	Hoop Stress (σ_θ)
130	130
110	110
65	130

2.4 Scanning Electron Microscopy and Electron Backscatter Diffraction

An FEI Magellan fitted with a NordlysNano EBSD detector and controlled by the AZTEC 4.3 software was utilised for both backscatter electron imaging (BSE) as well as Electron Backscatter Diffraction (EBSD). The BSE images were acquired at an accelerating voltage of 10 KeV and current of 0.8 nA where an insertable concentric backscatter (CBS) detector was used to maximise the BSE signal collection. To cover a statistically relevant area whilst retaining spatial resolution for clear hydride identification on each sample, image matrices (with many high magnification images) were captured using the FEI MAPS software, where a three-point focus interpolation was utilised to ensure focus across the sample. For EBSD, the following collection parameters were utilised: a beam current of 1.6 nA, accelerating voltage of 20 KeV and step size of 0.1 μm. The radial (RD) / Circumferential (CD) direction of the tube surface was imaged.

The orientation, connectivity and length of hydrides before and after reorientation were analysed using the python package HAPPy[300]. For each condition at least four micrographs were analysed such that a mean across the entire cladding could be obtained. To characterise the connectivity of the microstructure, the branch length fraction (BLF) and path of lowest cost (PLC) was computed such that the radial connectivity of the microstructure[300] could be visualised. Here, a high BLF is indicative of a high degree of hydride branching off the main chain of the hydride. The main chain is defined as the longest continuous hydride and a branch is anything connecting off this chain. Further, the path of lowest cost provides an indication of the plausibility of radial crack to propagation within the microstructure; a low cost suggests that through thickness cracking is highly plausible. For a more detailed description of these parameters please refer to [300]. During analysis, the distance weight parameter was set to 1.5 and min_feature_size was 20 μm. These parameters were kept constant across all samples.

2.5 X-Ray Diffraction

For the x-ray diffraction of the hydrided samples, a Rigaku SmartLab with a copper rotating anode, a germanium (220) double bounce incident monochromator, and a HyPix-3000 single photon counting 2D pixel array solid state detector was used. Instrumental effects were taken into account with an LaB_6 instrumental pattern. The sample to detector distance was 300 mm, the measurements were conducted over a 25-85° range and the scan speed was 0.1°/min. The convolutional multiple whole profile (CMWP) method[184,203] was used on these patterns to determine the dislocation density within the matrix and the hydrides.

2.6 Finite Element Analysis (FEA)

Finite element analysis modelling in Abaqus was conducted to compute the local variation in stresses for grains oriented in the $<11\bar{2}0>$ and $<10\bar{1}0>$ direction during cooling. Here a 2D model with a mesh size of 25 μm was created from which inferences about the relationship

between γ stability and grain orientation could be made. The difference in orientations was simulated by rotating the grains by 30 ° along the axial direction (AD). The stress and thermal expansion coefficients input into the model accounted for the highly anisotropic nature of Zr stemming from its hexagonal crystal structure. Importantly, only expansion along the a-direction was simulated as the effects of the c-direction for both grain orientations was deemed to be quite similar and therefore was not considered in this study. Table 3 details the elastic properties that were input into the model. The coefficient of thermal expansion utilised was α_{11} = 9.5 E-6 deg^{-1}.

Table 2.3 Elastic Properties input into the FEA model, where E and G are the elastic and shear moduli respectively.

	E1 (MPa)	E2 (MPa)	Poisson's ratio	G12 (MPa)
Elastic properties	1.562E+5	1.746E+5	0.32	6.448E+4

To account for any plastic effects during cooling, stress strain curves at room temperature and 400 ºC were extrapolated from Lee et al's study [301]. The variation in plastic properties with temperature upon cooling was estimated by a linear interpolation function. During the initial step a predefined field was used to establish a starting temperature of 400 ºC, this was followed by a coupled displacement-temperature step where a second predefined field was applied to reduce the temperature down to 20 ºC. Boundary conditions were applied so that the western and southern faces were restricted to zero displacement in the x and y direction respectively. A key assumption made was that at 400 ºC there was zero stress within the microstructure. This enabled a simpler more computationally efficient model to be developed. Importantly, the stresses at this temperature were not significant for this study, but rather the influence that cooling had on altering the stress state of the microstructure was of interest.

3. RESULTS

3.1 HYDRIDE PRECIPITATION

In this section, the results pertaining to hydride precipitation and the influence of microstructural features on the morphology and orientation of the hydrides is presented.

3.1.1 RELATIONSHIP BETWEEN MICROSTRUCTURE AND HYDRIDE ORIENTATION

Optical micrographs of the four different metallurgical conditions after hydriding are shown in Figure 3.1. It is immediately apparent that the size, morphology and distribution of the hydrides substantially varies with microstructural condition. In the stress-relieved and partially recrystallised samples (485 °C and 520 °C), connected hydride platelets are aligned over a relatively long distance in the circumferential direction (CD), whilst in the fully recrystallised samples, hydride platelets are connected over a shorter distance and display a greater spread in orientations.

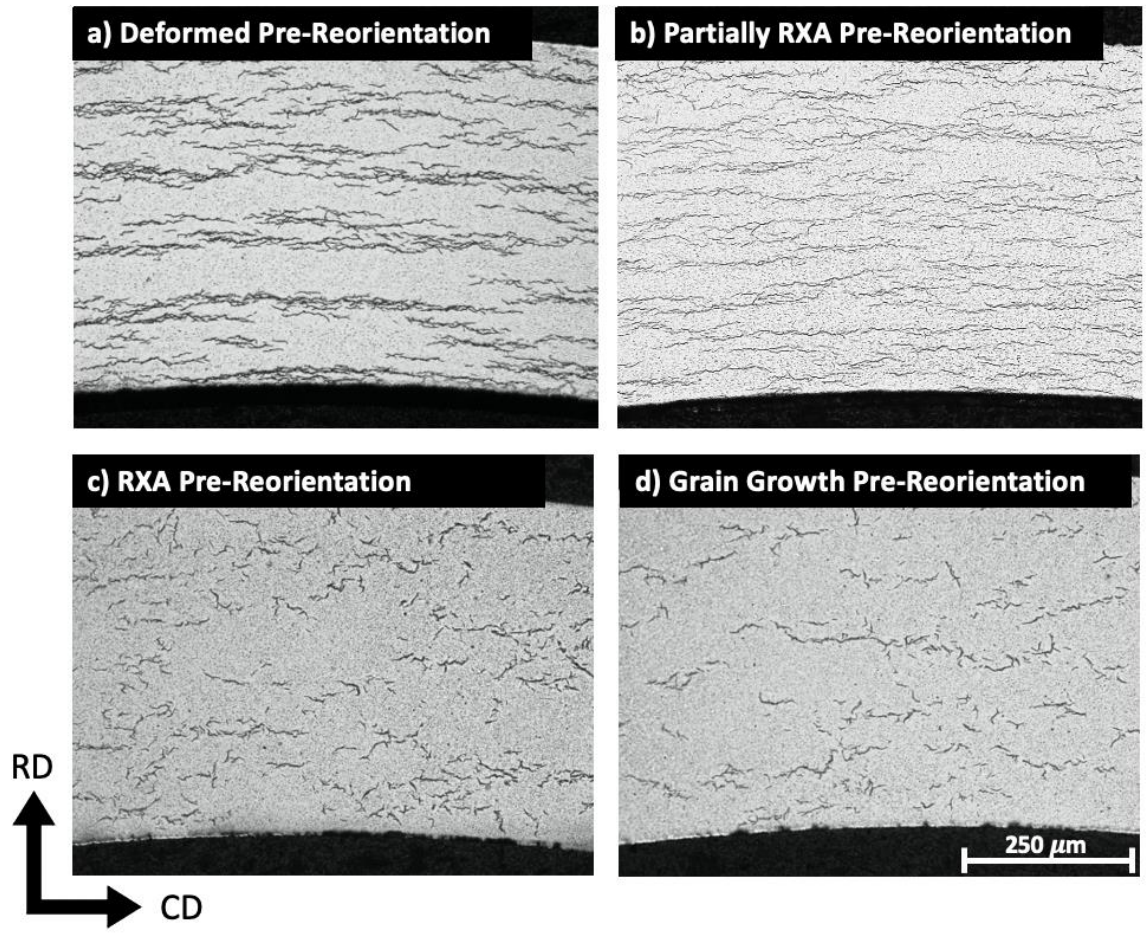

Figure 3.1 Optical micrographs of the hydrided specimen at the four different metallurgical states a) 485 ºC, b) 520 ºC, c) 560 ºC, d) 730 ºC. A stark difference in the size, morphology and orientation between the metallurgical states is apparent, whereby the fully recrystallised samples have smaller, more dispersed hydrides with a greater range in orientations when compared to the cold-worked and partially recrystallised samples.

Furthermore, more quantitative analysis of the hydride parameters, Figure 3.2, can be carried out. Figure 3.2a plots the grain aspect ratio (obtained from EBSD analysis) and Figure 3.2b plots the dislocation density (obtained from CMWP analysis) together with the radial hydride fraction (RHF) for the four metallurgical conditions identified by their final heat treatment temperature. The grain aspect ratio was used here as a measure of the extent of recrystallisation within the microstructure, where a value close to one is equivalent to a fully recrystallised state. Additionally, the RHF for at least four micrographs for each condition was calculated such that an average and standard deviation value could be attained.

From Figure 3.2a, an inverse trend can be observed between the grain aspect ratio and the RHF, with elongated grains (elongated along the CD) showing practically no radially aligned hydrides. Conversely, as the aspect ratio is reduced and tends towards 1 the RHF increases by around 10%. Moreover, Figure 3.2b highlights that the dislocation density and RHF are also inversely related, such that when the dislocation density is around $10^{14}\,m^{-2}$ in the stress relieved state, the RHF is 0.5%, whereas when the dislocation density is close to 0, the RHF increases to around 10%. Both of these parameters highlight that the metallurgical state of the microstructure already dictates the extent of radial hydride formation before any external stress is applied.

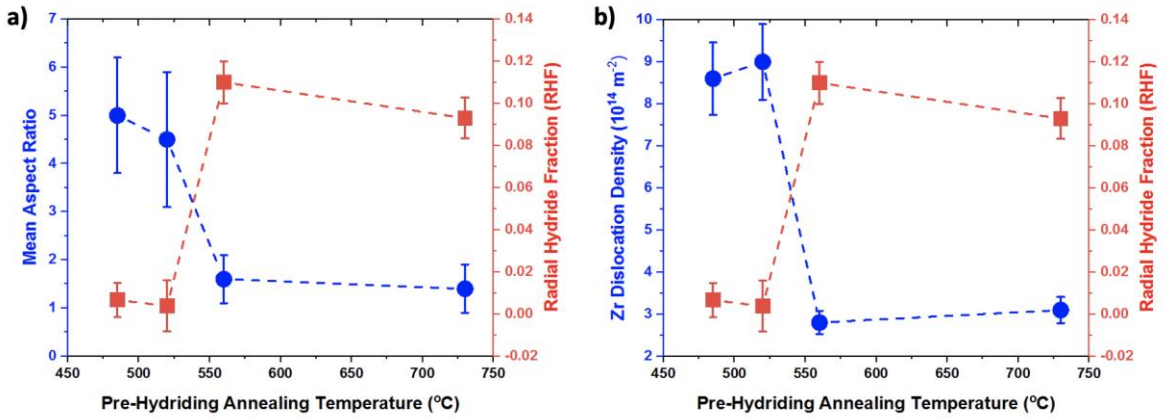

Figure 3.2 Influence on microstructural features during hydride precipitation where a) plots the grain aspect ratio and RHF as a function of metallurgical state and b) displays the dislocation density and RHF as a function of temperature.

3.1.2 RELATIONSHIP BETWEEN THE METALLURGICAL STATE AND HYDRIDE PHASE

With an increased number of studies reporting the stability of the γ phase at room temperature [91,106,109,110], the influence of the metallurgical state in promoting its stability was explored in this section. It is important to note that, as identified by Tulk et al. [103], the difference in yield strength for different metallurgical states could alter the stability of the γ phase within the microstructure. Therefore, the prevalence of the γ phase in the stress-relieved and recrystallised material was explored.

A recently developed technique by Maric et al.[302] was used to distinguish between the δ and γ phases. Dictionary indexing in conjunction with orientation relationship analysis from EBSD data provided insight into the prevalence and distribution of these hydride phases in the stress-relieved and recrystallised material. Figure 3.3a,d plot the phase maps for hydrides at the two metallurgical states, wherein the lack of γ phase in the stress-relieved state is immediately apparent. Figure 3.3a,d also highlight that the stress-relieved state contains a greater number of smaller intra-granular hydrides. This could be due to hydride precipitation on dislocations within the deformed grains.

The hydride IPF maps in Figure 3.3b,e highlight that the recrystallised sample has a prevalent γ fringe at the Hydride/Zr phase boundary whilst the orientations of the hydrides in the stress-relieved microstructure are much more dispersed and no γ fringe can be identified. It is interesting to note that when correlating the matrix orientations in Figure 3.3c,f to the prevalence of γ hydride, in both the stress-relieved and recrystallised microstructures, there appears to be no γ hydride formation on grains oriented in the $<10\bar{1}0>$ direction. Reasons for this will be proposed in the discussion. The authors highlight that it is unlikely that the prevalence of this γ fringe structure is an artefact, as many different maps of several regions of the microstructure were collected all exhibiting this fringe like structure (see Figure 7.3 of the supplementary information for another example). However, to further address and affirm this TEM studies visualising the fringe and establishing crystallographic relationships should be conducted.

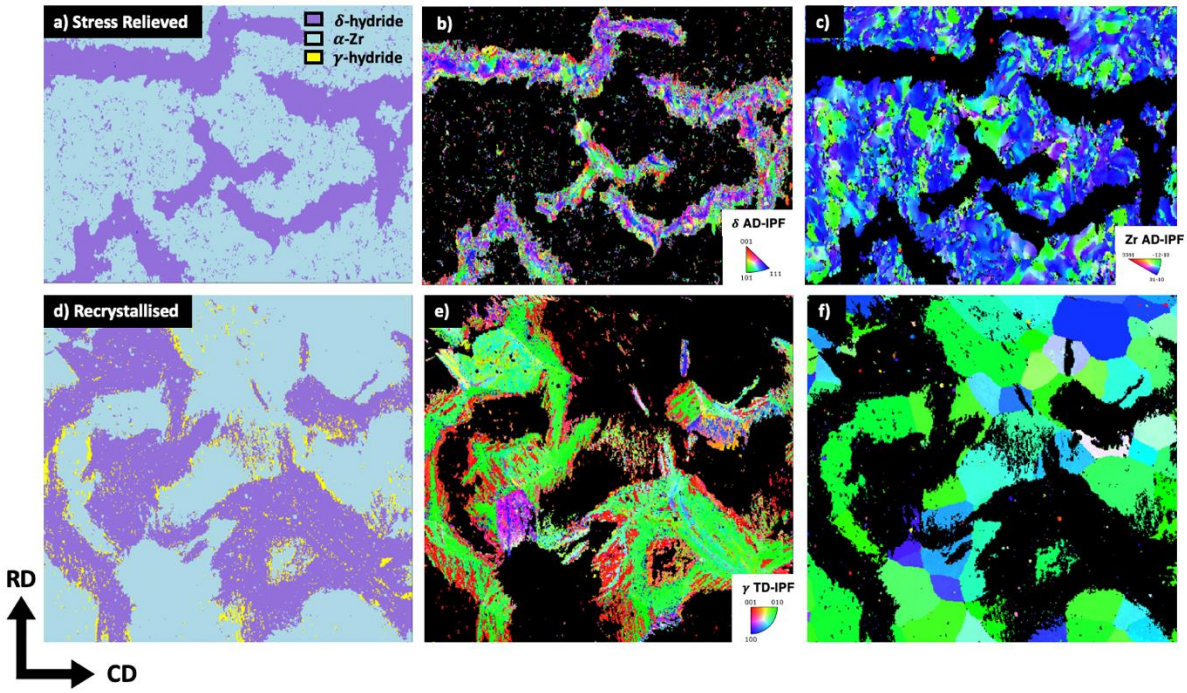

Figure 3.3 EBSD a,d) phase map of the stress relieved and recrystallised microstructures respectively highlighting the presence of gamma in the recrystallised but not stress relieved microstructure. b,c,e,f) IPF orientation maps of the hydride and matrix grains whereby the red δ and γ fringe in the recrystallised material is apparent.

3.2 HYDRIDE REORIENTATION

3.2.1 EVOLUTION OF RHF WITH STRESS AT DIFFERENT METALLURGICAL STATES

Large scale BSE maps were taken of the entire cross section of cladding tubes to investigate the extent of reorientation for each heat treatment temperature. Firstly, as shown by the BSE maps in the supplementary information (Figure 7.3), the extent of radial hydride precipitation remains constant across the entire cross section, suggesting a homogenous applied stress condition for this section of the tube.

Figure 3.4 plots sections of the BSE maps taken for each metallurgical state at a stress of σ_z = 130 MPa, σ_θ = 130 MPa. Here it is apparent that extensive hydride reorientation occurs in all samples regardless of the metallurgical state. The micrographs demonstrate qualitatively that the stress-relieved sample has the greatest degree of radial hydrides when compared to the other three conditions. However, in those conditions the hydrides appear to be more interconnected from the top to the bottom of the cladding tube. The other two applied stress conditions revealed qualitatively similar results and are shown in the supplementary material. Figure 7.2 also demonstrates this for the partially recrystallised microstructure stressed to the three different conditions.

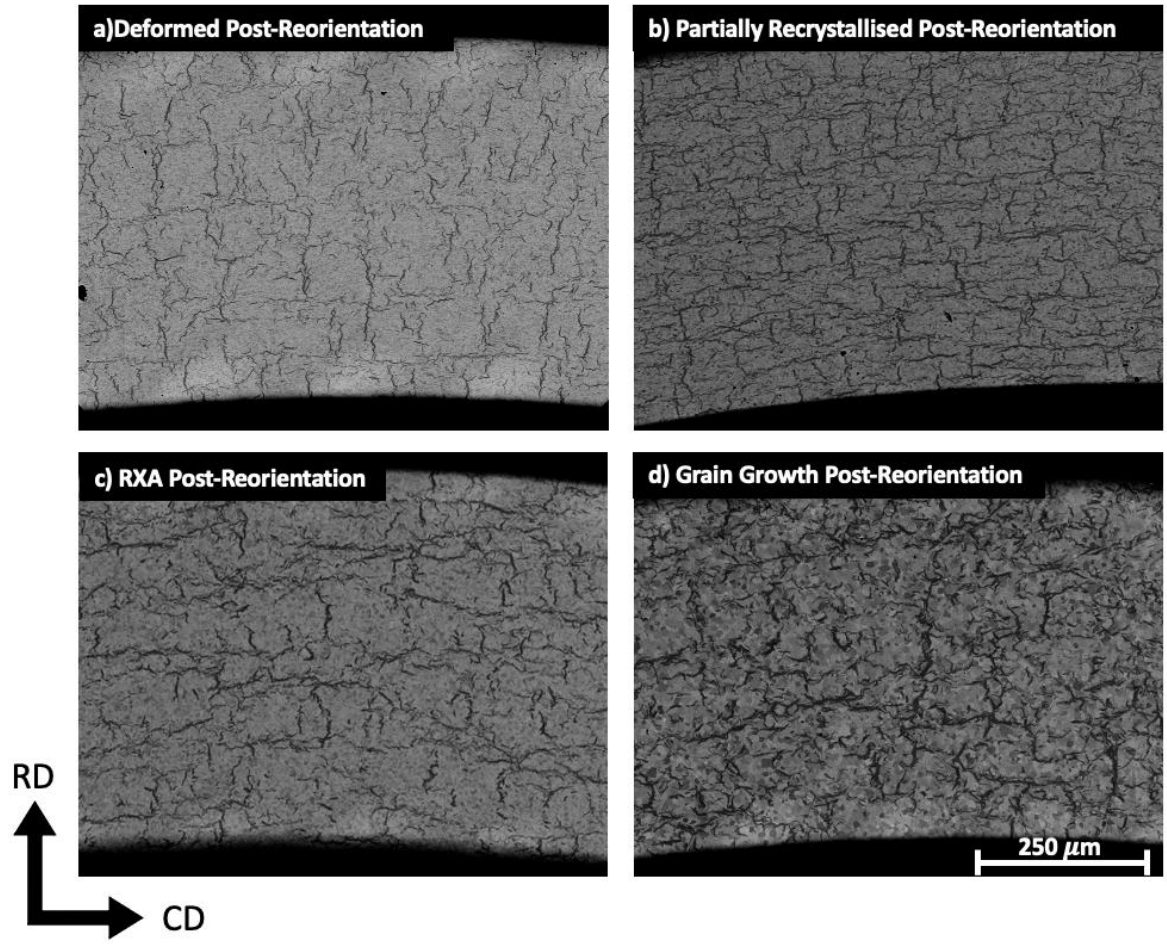

Figure 3.4 BSE micrographs of the hydrided specimen after being subject to reorientation testing at a stress of σz = 130 MPa σθ = 130 MPa for the four different metallurgical states a) 485 °C, b) 520 °C, c) 560 °C, d) 730 °C. It is immediately apparent that reorientation has occurred for all samples under this stress. It appears that the extent of radial hydride formation is the greatest for the 485 °C whilst the other samples seem to have a greater mixture of both circumferential and radial hydrides.

Quantification of the connectivity and orientation of the hydrides was conducted and is shown in Figure 3.5. Here, quantitative analysis of RHF, hydride length and hydride connectivity for each metallurgical state before and after reorientation using the HAPPy analysis tool was conducted. Figure 3.5a demonstrates that once the samples have undergone any thermomechanical cycle at all three stresses, the RHF has increased to at least 20% though it is significantly higher for the stress-relieved condition. There is a slight tendency that the highest biaxial stress condition generates the greatest RHF, which is most evident for the stress-relieved microstructure.

Figure 3.5b highlights that for the stress-relieved and partially recrystallised microstructures the mean hydride length is high before the thermomechanical cycle, while for the fully recrystallised conditions the mean hydride length is reduced by 25 %. On the other hand, after the thermomechanical cycle, the mean hydride length is the lowest for the stress-relieved condition (30-50 μm dependent on the applied stress) and is now higher for the other three metallurgical states (>60 μm). The stress biaxiality seems to play no significant role for the range of stresses considered, with a difference of less than 0.1 in the RHF and 10 μm in the hydride length observed.

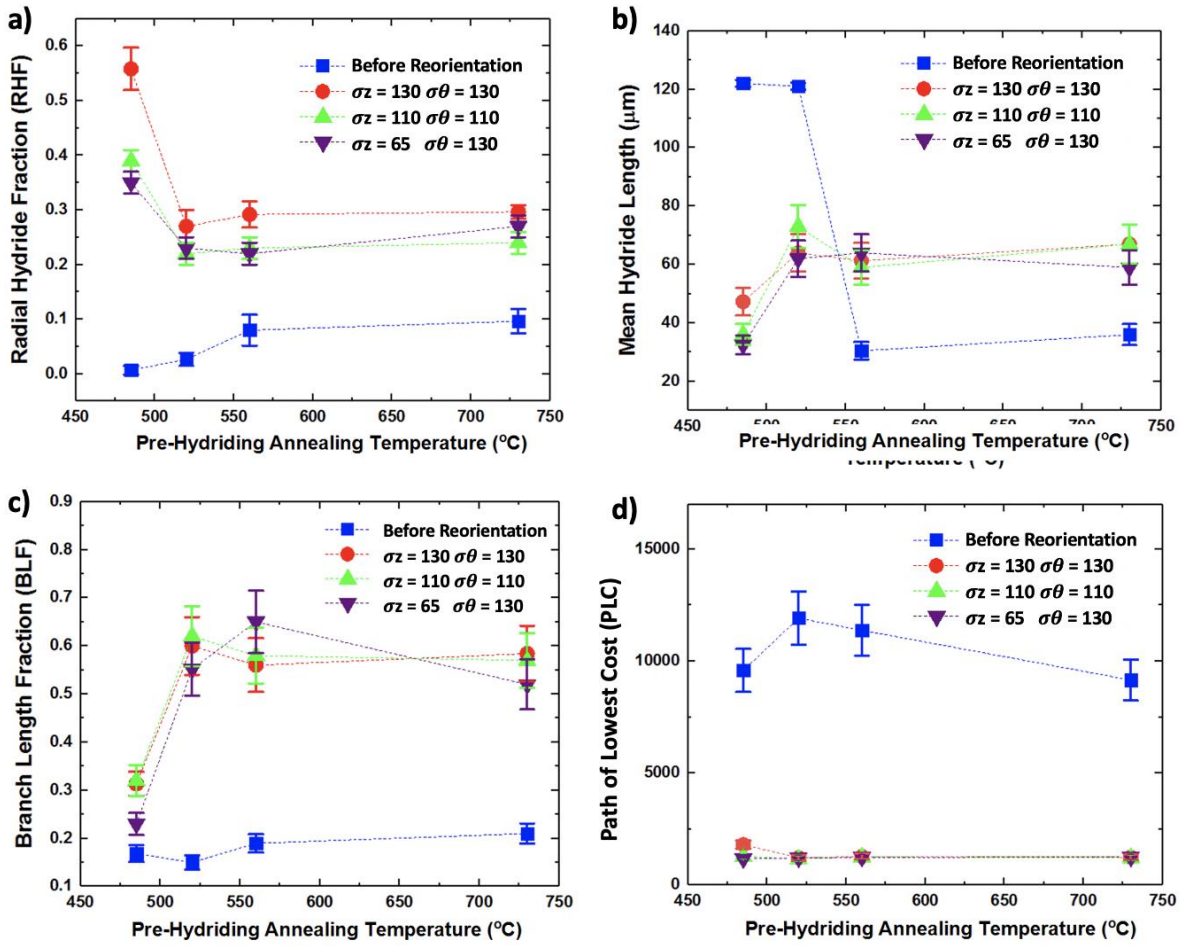

Figure 3.5 Evolution of the a) RHF, b) Mean Hydride Length, c) Branch Length Fraction (BLF) and d) Path of lowest cost (PLC) for the unstressed and three different reorientation stresses at different metallurgical states. Here it can be seen that the RHF for all three stresses is much higher than for the un-stressed sample and is the greatest for the stress-relieved sample. The RHF appears to remain quite constant for the other three metallurgical states. The mean hydride length for the pre-reoriented appears to shift from high to low whilst it remains quite constant for the samples post-reorientation. In general from c,d) it is apparent that a high BLF yields a low PLC, suggesting that the hydrides within the microstructure are highly connected. The exception to this is the stress-relieved sample which has a low BLF and low PLC.

Figure 3.5c and d show the branch length fraction (BLF) and path of lowest cost (PLC) for the different microstructure conditions before and after the various thermomechanical cycles. From Figure 3.5c,d it becomes immediately apparent that for the initial conditions (before reorientation) the BLF and PLC are around 0 and greater than around 10000, respectively. This suggests that hydride-related through thickness crack propagation is minimised due to the predominantly circumferential arrangement of the hydrides. On the other hand, after any of the thermomechanical cycles, the BLF increases to around 0.6 and PLC drops close to zero for the partially and fully recrystallised conditions. This indicates that for these three conditions interconnected hydride chains aligned in the radial direction of the cladding have formed such that crack formation and propagation in the through thickness cladding is likely. Interestingly, the BLF for the stress-relieved condition has changed less dramatically after the various thermomechanical cycles but the PLC still drops to close to 0. This could indicate that when the RHF is high, separate radial hydride chains form extensively within the microstructure such that a continuous path along the hydrides can form in the radial direction and cause significant damage without the need for substantial branching.

3.2.2 DISLOCATION EVOLUTION DURING PRECIPITATION AND REORIENTATION

The influence of hydride precipitation and reorientation on the dislocation density of the Zr matrix as well as the hydride phase are shown in Figure 3.6 where in a) the pink squares, green circles and black triangles are the matrix dislocation density before hydriding the material, after hydriding and after the thermomechanical cycle, respectively. It is important to note here that the samples in the As-received condition have been heat treated to the respective pre-hydriding annealing temperatures only. No hydrogen or further heat treatments were done to these samples. Figure 3.6b plots the dislocation density of the δ hydride before and after thermomechanical processing in green and black respectively.

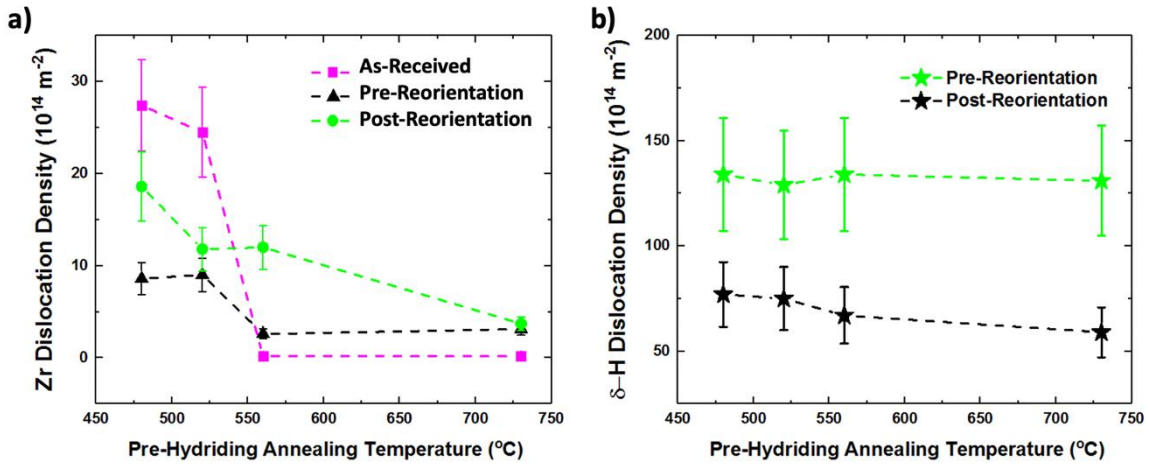

Figure 3.6 The evolution of a) Zr and b) δ-Hydride dislocation density during hydride precipitation and reorientation at different metallurgical states. In a) the increased time at elevated temperatures during hydriding and reorientation has resulted in an overall reduction in the dislocation density for the Zr matrix, particularly in the 485 °C and 520 °C sample. Further, for all cases containing hydrides, the dislocation density in the matrix is higher after reorientation. B) highlights that the dislocation density within the hydride is higher before hydride reorientation has occurred.

Figure 3.6a shows that the hydriding process at 400 °C for 3.5-10 hours does significantly reduce the dislocation density for the stress-relieved and partially recrystallised condition by at least 20 E14 m^{-2}. Further, it is apparent that for all metallurgical states, the matrix dislocation density has increased after the thermomechanical cycle by at most 10 E14 m^{-2}. Figure 3.6b demonstrates a significant drop of dislocation density in δ hydrides as a result of the thermomechanical cycle. On average, the dislocation density in the δ hydride before and after reorientation for all metallurgical states is 130 E14 m^{-2} and 70 E14 m^{-2}.

Additionally, EBSD was conducted on samples of all metallurgical states before and after reorientation to characterise changes in orientation relationships (Ors), phases and grain misorientation due to the reorientation. As shown in Figure 3.6a, the thermomechanical cycles produced the greatest dislocation density change in the recrystallised condition for which detailed EBSD analysis is shown in Figure 3.7. EBSD maps from the other metallurgical states before and after the thermomechanical cycle can be found in Figures Figure 7.3 and Figure 7.4 in the supplementary material. Figure 3.7a-d and Figure 3.7b,e display IPF coloured orientation maps of the Zr matrix and hydrides showing the arrangement of both phases with hydrides being predominantly intergranular and displaying different crystallographic orientations.

Additionally, some transgranular hydrides, highlighted by red circles, are apparent and appear to mostly form on grains oriented in the <10$\bar{1}$0> direction. Figure 3.7c,f plot the 5x5 kernel average misorientation (KAM) before and after the thermomechanical cycle highlighting the high KAM values for the hydrides and the dramatic increase of KAM values in the matrix after the thermomechanical cycle. Both observations are in agreement with the results shown in Figure 3.6.

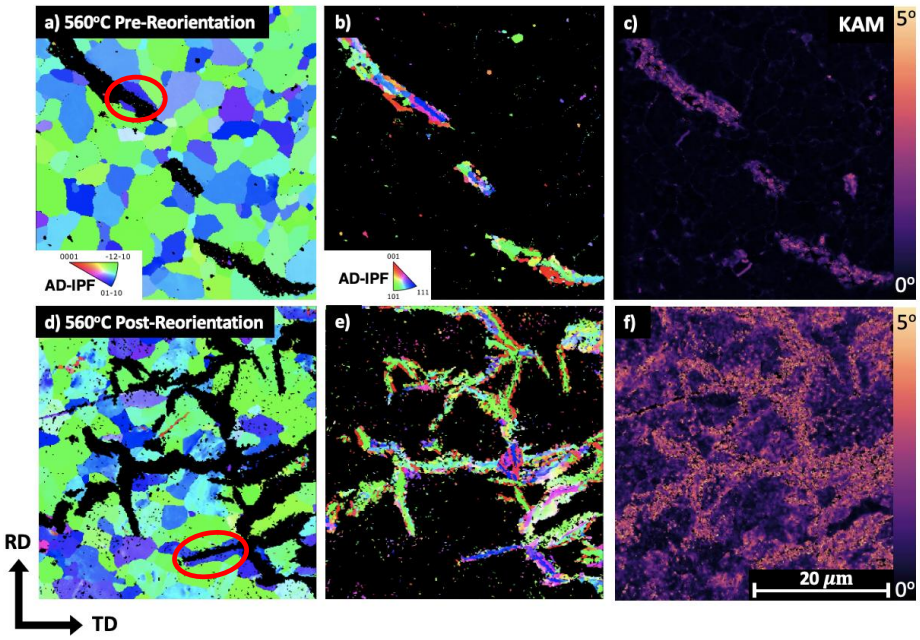

Figure 3.7 EBSD characterisation of the 560°C sample before and after hydride reorientation. A,d) depict AD-IPF maps of the Zr matrix, here the recrystallised, equiaxed grain structure before and after reorientation is apparent. B,e) show the AD-IPF maps of the hydride phase, here the varying orientations within the hydride can be seen. C,f) kernel average misorientation (KAM) maps for the samples before and after reorientation. Here the KAM within the hydride seems to be quite similar (i.e., high) whereas the Zr matrix before reorientation has almost zero KAM whilst after reorientation the KAM in the matrix appears to be greater.

To investigate whether the Ors made between the matrix and hydride are retained after reorientation OR analysis using pole figures was conducted. Figure 3.8 shows the orientation relationships formed between the hydride and the Zr matrix before and after the thermomechanical cycle. The γ and δ (as discussed by [264,288,302]) each form crystallographic orientation relationships with the Zr matrix. Maric et al. [299] and Kerr et al. [285] show that during stressed precipitation the OR of the δ hydride changes to better accommodate the increased stress from $\{0001\}_\alpha||\{111\}_\delta$ and $<11\bar{2}0>_\alpha||<110>_\delta$ to $\{0001\}_\alpha||\{001\}_\delta$ and $<11\bar{2}0>_\alpha||<1\bar{1}0>_\delta$ respectively. These Ors will be referred to as δ-major and δ-minor in this study respectively. Further, the OR that the γ hydride makes with Zr matrix is $\{0001\}_\alpha||\{001\}_\gamma$ and $<11\bar{2}0>_\alpha||<1\bar{1}0>_\gamma$, and is consistent with reports in literature[9,98,117,290,291]. It is evident from the EBSD analysis that the hydride Ors are retained after thermomechanical cycling providing further evidence in support of reorientation not being a crystallographic phenomenon[6,9,146].

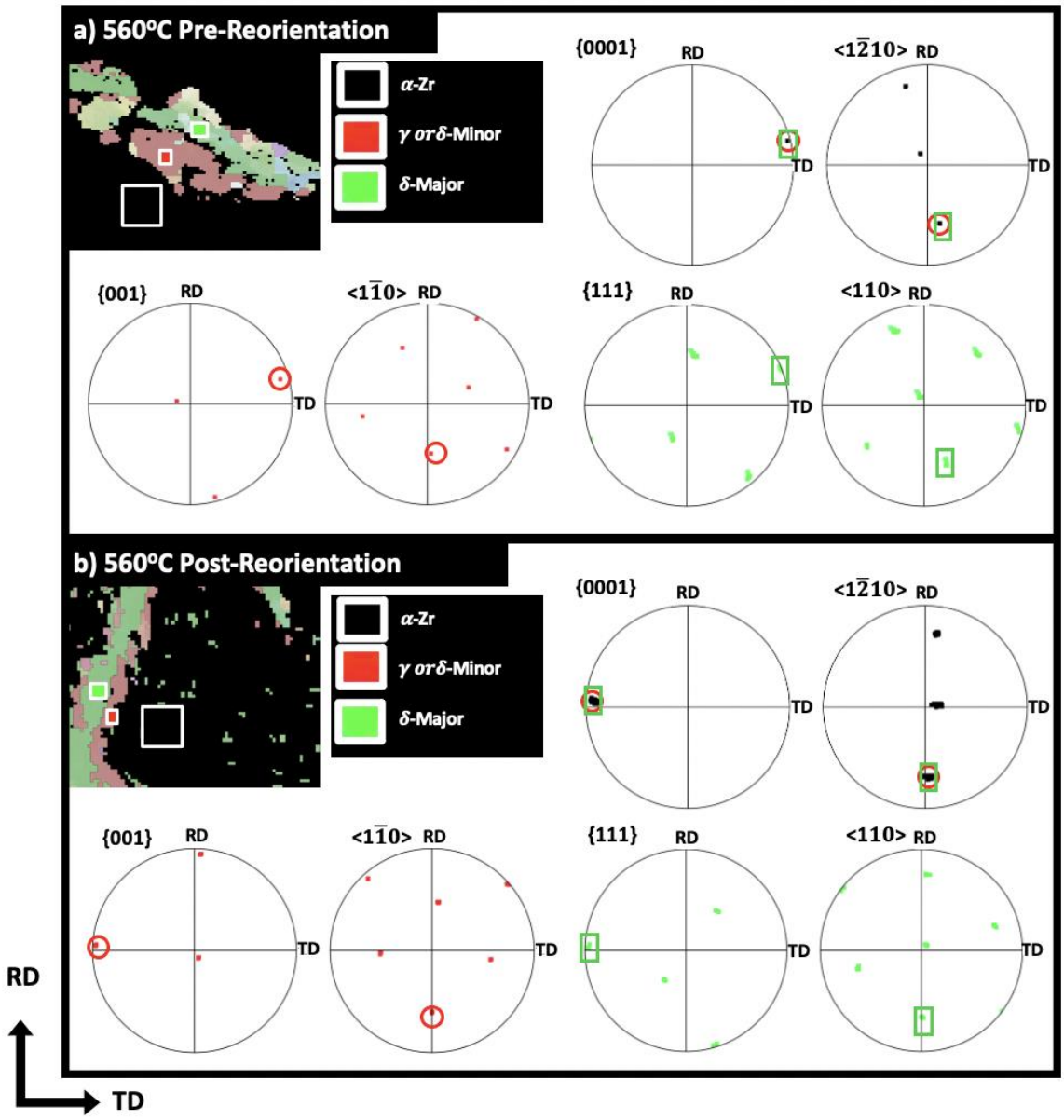

Figure 3.8 Orientation relationship analysis of the hydrides a) before and b) after reorientation. Here the scattered pole figures for the Zr, γ, δ-minor and δ-major orientation relationships are plotted in black, red and green respectively. Importantly, it is shown here that the orientation relationships that the Zr makes with the hydrides is retained and that the γ fringe appears to be prevalent before and after reorientation.

4. DISCUSSION

4.1 HYDROGEN PRECIPITATION UNDER NO STRESS

4.1.1 RELATIONSHIP BETWEEN METALLURGICAL STATE AND THE MORPHOLOGY AND ORIENTATION OF THE HYDRIDE PRECIPITATES

The microstructure induced at different metallurgical states has a significant influence on the length, morphology, and orientation of the hydrides as shown by the micrographs in Figure 3.1. Similar to studies by Une et al,[303] as well as Bai et al, [304] the stress-relieved microstructure contains long hydride chains oriented in circumferential direction whilst the recrystallised hydrides are on average much shorter and have a greater radial distribution. To understand the principal matrix microstructural features driving this drastic change in hydride morphology, the grain aspect ratio and dislocation density were plotted with the RHF at all four metallurgical conditions as shown in Figure 3.2. Here it is apparent that as the material recrystallises, i.e., the dislocation density and grain aspect ratio approach zero and one, respectively, the extent of radial hydride precipitation increases by around 10% and the mean hydride length is reduced to 90 μm.

This suggests that the morphology and orientation of hydride precipitation is strongly dependent on the metallurgical state of the material. To explore this further, AD-IPF orientation maps of the Zr matrix are shown in Figure 4.1. Here the stress-relieved, partially recrystallised, recrystallised, and recrystallised with substantial grain growth AD-IPF Zr maps are depicted. Figure 4.1a,b qualitatively affirms the generation of grains with high aspect ratios along the circumferential direction during the deformation process. It is apparent that at all metallurgical states, hydride nucleation and growth preferentially occurs on grain boundaries[6]. Grains with higher aspect ratios, have limited number of available sites for radial hydride formation such that precipitation of elongated circumferential hydride chains is promoted. During recrystallisation, as the aspect ratio of the grains reduces (as shown in Figure 3.2a and Figure 4.1c,d), the microstructure becomes populated with equiaxed grains. Here the radial and circumferential components of the grain boundary are equally likely such that both circumferential and radial inter-granular hydride precipitation under no external stress occurs.

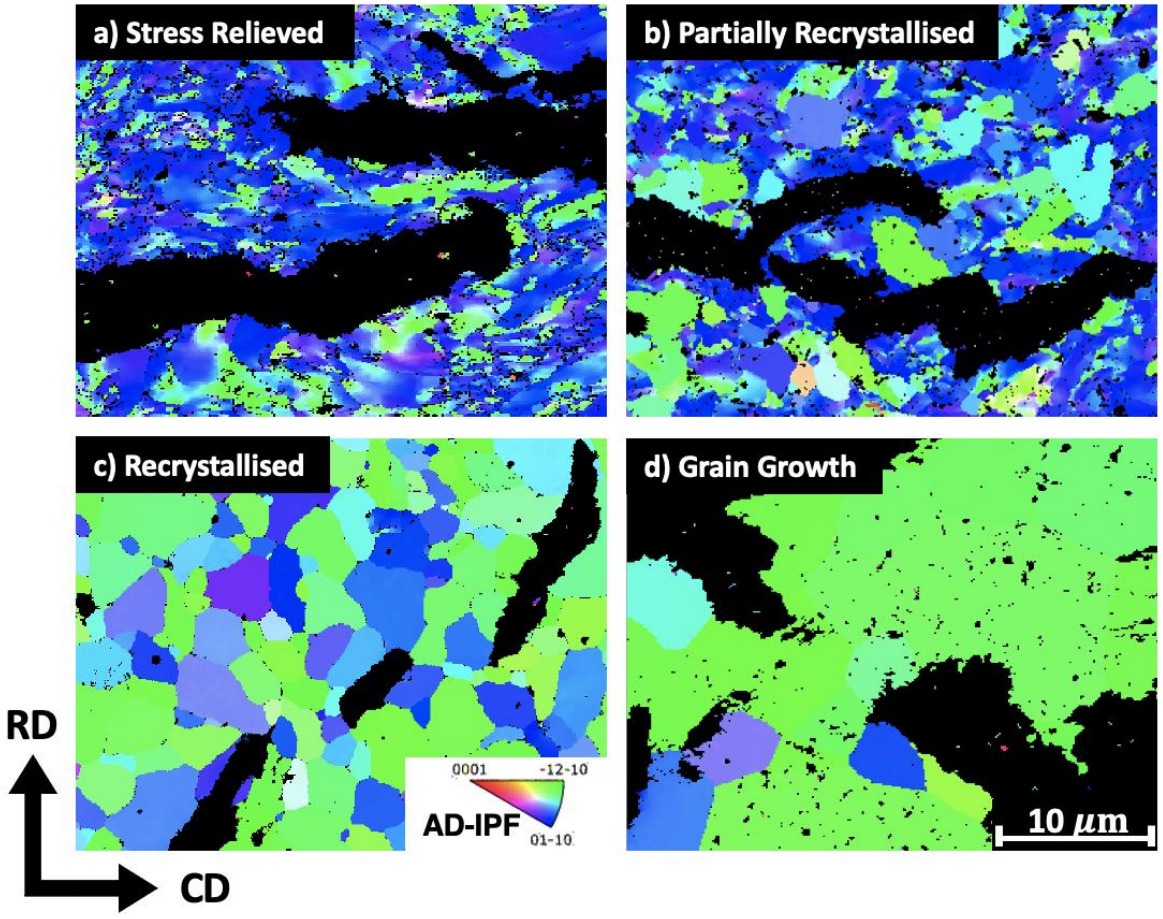

Figure 4.1 AD-IPF orientation maps of the Zr matrix grains at the four different metallurgical states a) stress-relieved, b) partially recrystallised, c) recrystallised and d) recrystallised with extensive grain growth. Here the stark difference in grain structure for the stress-relieved and recrystallised samples is apparent whereby the stress-relieved grains appear to be elongated in CD and have negligible radial components. On the other hand the recrystallised grains are equiaxed and have a very low defect density.

4.2 INFLUENCE OF METALLURGICAL STATE ON HYDRIDE PHASE STABILITY

There has been extensive debate with regards to the stability of the γ-hydride phase within the literature. Recently, substantial evidence has accumulated in support of the γ-hydride phase being the low temperature stable phase within Zr [88,91,96,100,106,109,110,267,268,305]. However, the factors promoting and inhibiting the stability of γ-hydride are still not clear. In this study, as shown in Figure 3.3, it is apparent that the metallurgical state of the matrix has a significant influence on the prevalence of γ-hydrides.

This could be due to, as highlighted by both Tulk et al.[103], and Cann et al.[108], the difference in strength between the stress-relieved and recrystallised samples wherein the reported yield strengths are 836 MPa and 440 MPa respectively[271,272]. In Tulk et al's.[103] work, the evolution of the volume fraction of γ and δ hydride was studied during cooling of both stress-relieved and recrystalised Zircaloy-2, and it was shown that under identical cooling conditions and similar hydrogen concentrations, the fraction of γ was at least 50% higher in the recrystallised sample which is comparable to the EBSD observations in Figure 3.3.

The suppression of γ within the stress-relieved material was related to the extent of hydrogen enrichment within the γ (ZrH) and δ ($ZrH_{1.6\text{-}1.7}$) hydride phases. The lower stoichiometry of hydrogen in the γ phase when compared to the δ phase could mean that a greater volume of γ hydride is required to precipitate to consume all of the available hydrogen. This subsequently results in a greater volume change and therefore increased strain in the microstructure. The higher strength of the matrix material could therefore supress this formation and favour the formation of the δ phase whereby the volumetric strain of the precipitating unit cell is lower[103,104]. This could be a pivotal reason why the γ-phase is not extensively seen in alloyed Zr as a large proportion of such analysis has been done on reactor grade alloys that have undergone substantial deformation and hence have increased strength.

Interestingly, recent studies have highlighted the prevalence of δ hydride with a different OR to the one conventionally reported in literature[9,98,117,290,291]. δ hydride adhering to the δ-minor OR forms to accommodate the high strains generated during hydride precipitation in the Zr matrix. As highlighted by Kerr et al. [288] as well as Maric et al.[302] the OR of this phase is the same as the γ phase which is $\{0001\}_{\alpha}\|\{001\}_{\gamma,\delta-\text{minor}}$ and $< 11\bar{2}0 >_{\alpha}\|< 1\bar{1}0 >_{\gamma,\delta-\text{minor}}$ respectively. Differentiation between the δ phase adhering to the δ-minor OR and the γ phase can be computed using dictionary indexing of Kikuchi patterns, whilst the difference between the two variants of the δ phase can be identified by the different ORs that these two phases make with the matrix as discussed by Maric et al.[302]. Figure 3.3e highlights that the <001>AD δ fringe forms with a distinctly different OR with the matrix when compared to the bulk δ with the δ-major OR to accommodate for the increased matrix strain during hydride precipitation upon cooling[288].

Upon closer inspection of the recrystallised sample that has been subject to substantial grain growth, it becomes apparent that both δ phase (adhering to the δ-minor OR) and γ hydride formation is supressed in grains of the $<10\bar{1}0>$ orientation and enhanced within the $<11\bar{2}0>$ oriented grains. Examples of this are shown in Figure 4.2. Here, a,d,g shows the IPF map for the Zr matrix and b,e,h shows the IPF map for the hydride phases at the same region. Figure 4.2 c,f,i plot the phase maps for the regions as well as the ORs made between the hydrides and the Zr matrix.

It is evident that for the grains oriented in the $<10\bar{1}0>$ direction, the only hydride phase present at the phase boundary is δ, which follows the δ-major OR. On the other hand, for grains oriented in the $<11\bar{2}0>$ direction, both γ and δ adhering to the δ-minor OR appear to have formed at the phase boundaries indicating their higher stability in grains of this orientation.

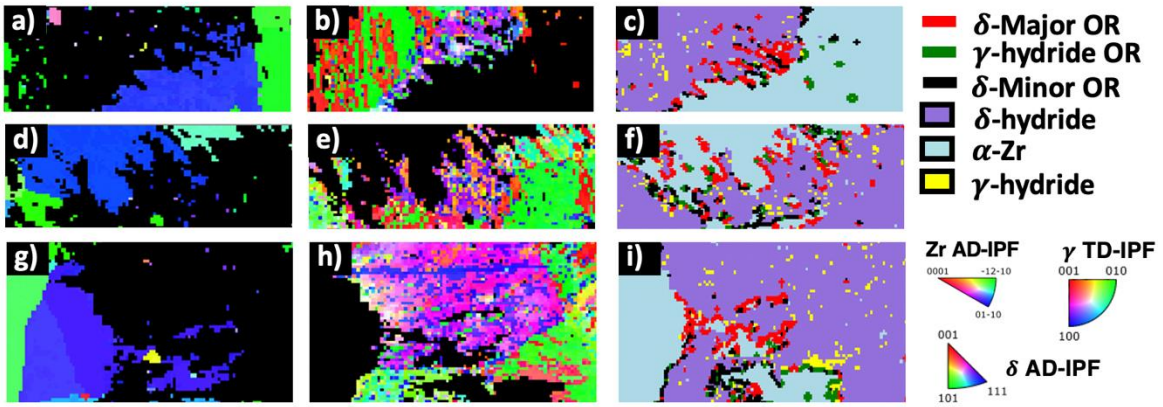

Figure 4.2 Depicts the stability of the δ phase on grains oriented in the <10-10> direction and the stability of the γ phase for the grains oriented in the <1-210>. a,d,g) IPF maps for the Zr matrix b,e,h) IPF maps of the hydride and c,f,i) Phase maps wherein the δ-hydride, γ-hydride and Zr are shown in purple, yellow, blue.

It is not immediately apparent how the difference in grain orientation influences the stability of the γ phase. To explore this, it is firstly important to identify the origin of these two distinct orientation fibres. Bozzolo et al.[42,43,221] and Maric et al.[306] highlight that during recrystallisation, a 30 ° rotation along the AD causes the observed change in grain orientation. Therefore, to understand the differences in hydrostatic stress states for these two grain orientations during cooling, a finite element analysis (FEA) model was created in Abaqus. FEA was specifically utilised in this study as it enabled us to generate a substantially sized microstructure consisting of many grains and was representative of an actual microstructure. A local orientation was able to be assigned to particular grains such that the 30 º shift between the <10$\bar{1}$0> and <11$\bar{2}$0> grain orientations could be simulated. This enabled the local stress variation upon cooling due to orientation differences to be calculated and understood. From these results inferences about the hydride phase stability for specific grain orientations could be made. As shown in Figure 4.3a, a simplified 2D model of a hexagonal microstructure consisting of the two respective grain orientations was simulated. The green and white grains represent the grains oriented in the <10$\bar{1}$0> and <11$\bar{2}$0> direction.

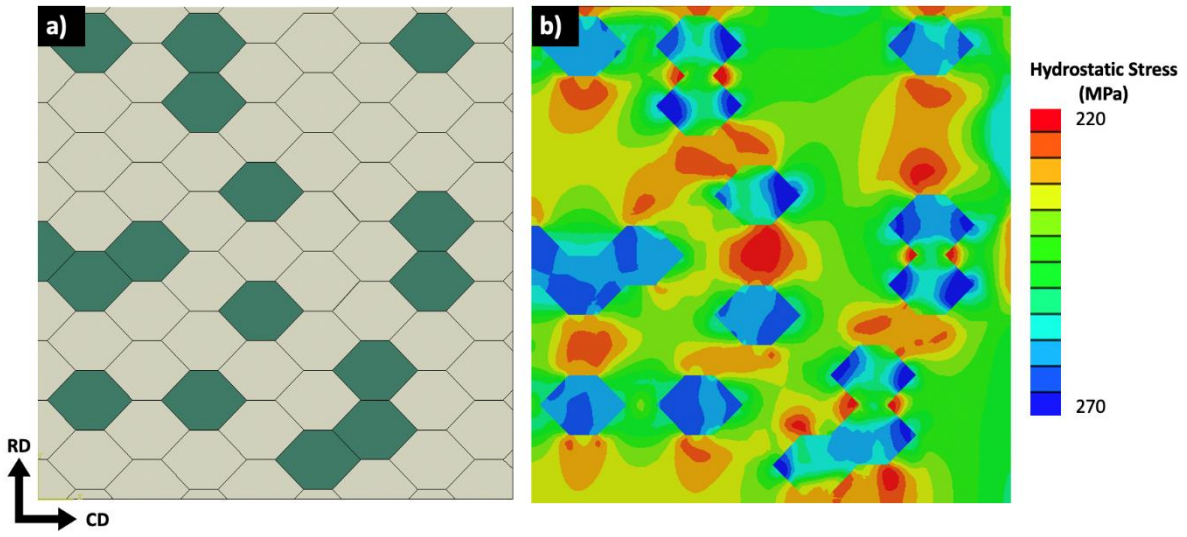

Figure 4.3 Finite element analysis model to understand the differences in stress in the grains oriented in the <10-10> and <11-20> direction as shown by the green and white grains in a respectively.

Figure 4.3b displays the hydrostatic stress states of both grain orientations after cooling from 400 °C. When comparing the grains oriented in the $<10\bar{1}0>$ and $<11\bar{2}0>$ direction, it is apparent that the $<10\bar{1}0>$ grains are predominantly in a compressive stress state. The high compressive stress could explain the suppression of the γ phase within these grains. To understand this better, it is important to note that when considering the magnitude of volumetric expansion of a single unit cell of γ and δ, the expansion of the γ is higher. Whereby, if we consider γ to be thermodynamically stable at room temperature, then the suppression of it is primarily controlled by the stress state of the microstructure. If the grain is in a state of compression, the higher volumetric expansion of the γ when compared to the δ phase is not favourable as greater work must be done to overcome the compressive stresses[307]. Therefore, it is more energetically viable for the δ phase to precipitate at these regions. On the other hand, when the grain is in tension (i.e., grains oriented in the $<11\bar{2}0>$ direction), precipitation of the γ phase can be better accommodated such that the thermodynamic driving force for its precipitation upon cooling is no longer supressed and encourages the formation of γ.

It is important to note that the transformation strain of hydrides is not purely isotropic. As such some shear components will need to be accommodated for. However, the shear component is much smaller than the hydrostatic component. Therefore, the influence of the hydrostatic stress components (as studied by the FEA model) in accommodating the hydride transformation strain is expected to dominate.

Therefore, the results highlight that γ phase stability seems to be dictated by both the local stress state and bulk mechanical properties of the Zr matrix. The complex nature of both the thermodynamic and material properties that drive the stability of this phase are highlighted in this work.

4.3 HYDRIDE REORIENTATION

4.3.1 METALLURGICAL STATE AND REORIENTATION

As shown in Figure 3.4, reorientation extensively occurs at all pre-hydriding metallurgical states, wherein the RHF is at least 25% greater in the samples after reorientation (Figure 3.5a). However, the greatest degree of reorientation has occurred in the stress-relieved sample. This is quantified in Figure 3.5a, where the RHF at all of the applied stresses in the stress-relieved samples is at least 10% greater than any of the other metallurgical states.

To understand this trend, it is important to consider the bulk hydrogen content of the samples relative to the solubility limit at a temperature of 400 ^{o}C for all metallurgical states. The hydrogen content in the stress-relieved condition is 200 ppm compared to at least 300 ppm in all the other metallurgical states. Therefore, during thermomechanical processing at 400 ^{o}C, as determined from the TSS_D equations detailed by McMinn et al.[73], the solubility of hydrogen in solid solution is around 180 ppm. Thus, for the stress-relieved material, unlike for the other three metallurgical states, almost all of the hydrogen will be in solid solution and will thus re-precipitate under stress upon cooling. This could explain the higher RHF values in the stress-relieved state when compared to the other conditions.

In the other three metallurgical states, when the hydrogen content is more comparable, there does not seem to be a prominent effect of the metallurgical state on the extent of reorientation. Here, as shown in Figure 3.5a, the RHFs are all similar. Additionally, unlike for the pre-reorientation samples, there is no distinct shift in RHF or mean hydride length for samples during recrystallisation. This suggests that the microstructural evolution during recrystallisation prior to hydriding does not have a substantial influence on the extent of reorientation. It is important to note that there could be a minor effect of metallurgical state on

the extent of reorientation which was not captured in this study because not all of the hydrogen was in solid solution during the thermomechanical cycle. However, the present results suggested that extrinsic factors such as the extent of applied stress will have more of an impact[8,10,145,153,157,158,163]. This is shown in the present study as the RHF is the largest for all metallurgical states that have been subject to the highest stress (σz = 130 MPa $\sigma\theta$ = 130 MPa).

From Figure 3.5c,d the significance of reorientation in promoting through thickness cladding cracking becomes immediately apparent. Here, for all metallurgical states, during hydride precipitation under no applied external stress, the branch length fraction (BLF) is negligible, and the path of lowest cost (PLC) is around 10 times greater than after thermomechanical loading. This suggests that through thickness cracking prior to hydride reorientation is highly unlikely. On the other hand, for the samples subject to thermomechanical processing, the interconnectivity of the hydride chains (as shown by the high BLF) as well as the greater RHF produces a microstructure that is highly susceptible to through thickness cracking. This is further supported by the low PLC (around 900) values for the samples after the thermomechanical cycle.

The mean hydride length plot in Figure 3.5b as well as the micrographs in Figure 3.4 highlight that after reorientation in the two recrystallised microstructures, the length of the hydride chains seems to have increased from 20 to 60 μm. This could be because, during reprecipitation, sympathetic nucleation of hydrides near the un-dissolved hydrides occurs such that the hydride chains appear to grow in circumferential direction even under an applied stress[308].

The stress-relieved sample has a significantly lower BLF than the other post-reorientation samples at different metallurgical states. This BLF is comparable to the pre-reorientation samples and could stem from the sample's lower hydrogen content. However, the low BLF does not seem to impact the PLC, whereby at a BLF of 0.3, the PLC is still only around 900. This suggests that at very high RHFs, an interconnected microstructure is not required to form a continuous brittle path along the radial direction of the tube. Here, the potency of increased RHFs even at lower hydrogen contents is highlighted.

4.4 EVOLUTION OF DISLOCATION DENSITY WITH HYDRIDE PRECIPITATION AND REORIENTATION

To understand the influence that hydride precipitation and reorientation has on the matrix and hydride phases, the dislocation density before hydriding, after hydride precipitation and thermomechanical processing was plotted for the matrix and hydrides in Figure 3.6.

During hydriding, the dislocation density within the matrix grains is substantially reduced. This initially seems counterintuitive, as it would be expected that the volumetric expansion due to hydride precipitation would result in substantial matrix deformation surrounding the hydride[309]. However, during the gas hydride charging procedure, the samples are heated to 400 $^{\circ}$C and held at this temperature for at least four hours. During this time, annealing of the microstructure occurs, promoting dislocation recovery[310]. Therefore, although an increase in matrix dislocation density occurs during hydride precipitation, it is not significant enough to balance out the reduction in dislocation density due to recovery.

When comparing the dislocation density in the matrix after hydriding, it is apparent that the dislocation density is substantially higher after reorientation. This suggests that during the reorientation process, even if some further microstructural recovery occurs due to the elevated temperatures, the dislocations induced in the matrix during hydride reorientation are significant enough to be identified. It is important to note that the increased matrix dislocation density is

unlikely to be due to the applied stress during reorientation, because even at 400 ^{o}C, the applied stress is at least three times lower than the yield stress in both the axial and hoop direction of the cladding tube[311]. Therefore, the observed increase is primarily due to the deformation of the matrix to accommodate the hydrides during re-precipitation. This is further confirmed in by the KAM maps shown in Figure 3.7, where the increase in matrix KAM particularly near precipitated hydrides after reorientation is shown.

Figure 3.6b plots the dislocation densities in the hydride phase before and after reorientation. The pre-reorientation hydride dislocation densities are consistent with those previously reported in literature[312]. No study to date has compared the evolution of the dislocation density before and after thermomechanical cycling. Here, the significantly higher dislocation density for all metallurgical states during hydride precipitation under no external stress is immediately apparent. A small contribution to this effect could be that the volumetric expansion that occurs during hydride precipitation in Zr is what drives the increased dislocation density in the matrix and hydride. For δ hydride precipitation, the volumetric expansion is reported to be around 17%[107,278]. In an unstressed matrix during hydride precipitation, the hydride precipitate expands into the matrix subsequently deforming both the surrounding matrix and hydride. However, during reprecipitation under a stress (both axial and hoop) the volume of the matrix is increased (even if just elastically). As a result, during re-precipitation the relative volume change required for hydride precipitation is reduced. However, elastic contributions are very small and cannot purely account for the very large difference in dislocation density observed. Another potential theory could be that the presence of the dislocation nests left behind after initial hydride precipitation and dissolution could provide more space for the hydride to precipitate into. The prevalence of these dislocation nests after dissolution and the strong tendency for hydride reprecipitation at these sites has been investigated and proven in a recent study by Long et al[148]. A schematic summarising the proposed effect is shown in Figure 4.4. Here in a) the initial matrix deformation due to hydride precipitation is shown. During dissolution, as shown in b) a nest of dislocations is left behind where the hydride used to be. This region could provide more space for the hydride to reprecipitate into under a load (d) resulting in better hydride accommodation and hence a lower dislocation density.

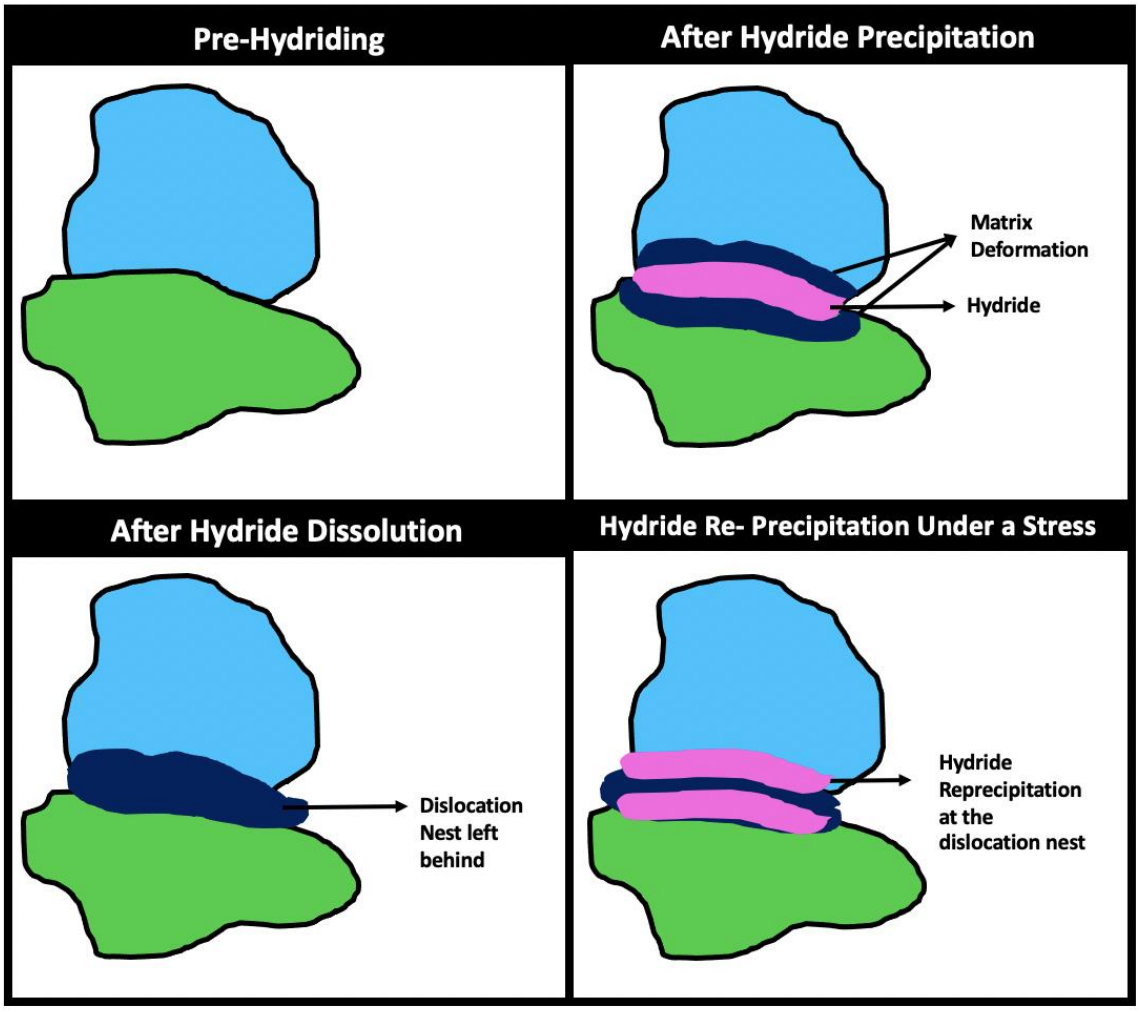

Figure 4.4 Schematic of the model developed to account for the reduced dislocation density in the reoriented samples when compared to the precipitated hydrides under no stress. Here, during hydride dissolution, a dislocation nest is left behind which provides greater space for the hydride to re-precipitate into resulting in better accommodation and hence a reduced hydride dislocation density value.

5. CONCLUSIONS

In this study, the influence of the metallurgical state on the morphology, phase stability and orientation of hydrides during precipitation and reorientation was explored. It was highlighted that the metallurgical state of the matrix has a significant influence on hydride precipitation whereby the extent of recrystallisation controls the distribution and orientation of precipitating hydrides. It was shown that the stress-relieved structure, which consists of elongated grains aligned in the CD of the tube, were shown to favour the precipitation of circumferential hydrides. On the other hand, the equiaxed grains in the recrystallised samples lead to the precipitation of shorter hydrides oriented in both the radial and circumferential direction. The reduction in yield strength during recrystallisation was shown to promote the stability of the γ phase. This effect was suppressed in the stress-relieved microstructure due to its increased strength. Further, in the recrystallised microstructure, the γ phase stability was shown to be related to hydrostatic stress state of grains oriented in the $<10\bar{1}0>$ direction

Unlike for hydride precipitation, the metallurgical state of the microstructure prior to hydriding seemed to have minimal influence on the extent of hydride reorientation. Here, no significant

shifts in RHF and mean hydride length were observed as the extent of recrystallisation within the matrix microstructure was increased. This provides strong evidence that the reorientation process is strongly driven by extrinsic factors such as applied stress rather than the microstructural features of the matrix.

Finally, the evolution of dislocation density in the matrix and hydride during both hydride precipitation and reorientation was investigated. It was highlighted that matrix annealing during hydriding is substantial enough to cause a reduction in dislocation density which overshadows the increase in dislocation density that results from the precipitation of hydrides in the matrix. On the other hand, during reorientation no further significant recovery occurs resulting in increased dislocation density within the matrix during hydride precipitation. Additionally, the evolution of the hydride dislocation density before and after reorientation was quantified whereby the δ hydride dislocation density before reorientation was a factor of two greater than after reorientation. To explain this, a model was developed to account for the reduced deformation of the hydride during precipitation under the application of an axial and hoop stress.

6. ACKNOWLEDGEMENTS

The Authors would like to thank Framatome for funding and providing the material for the present study. Philipp Frankel acknowledges support from MIDAS (EPSRC EP/SO1720X).. The authors thank Jean-Paul Vassault and Julien Augereau for sample preparation and experiments follow-up, Mariano Marini for hydriding the samples, and Sylvain Duval for reorientation tests. The research used UKAEA's Materials Research Facility, which has been funded by and is part of the UK's National Nuclear User Facility and Henry Royce Institute for Advanced Materials.

7. APPENDIX

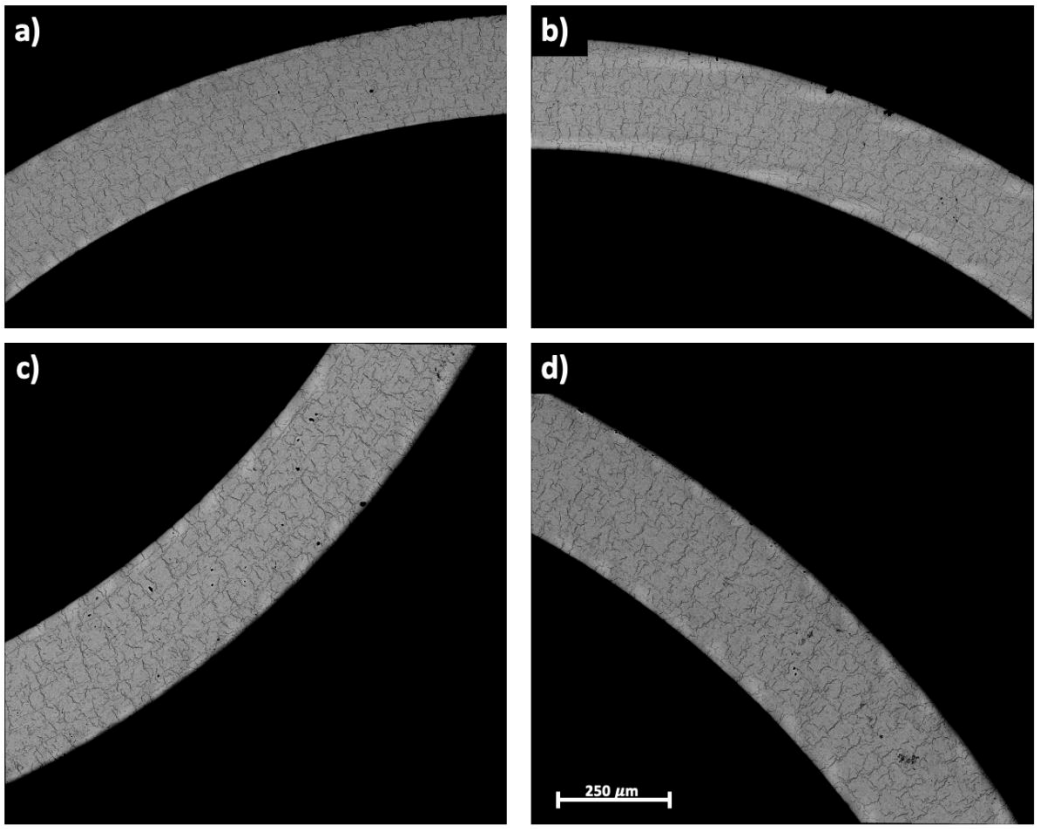

Figure 7.1 Evolution of the hydride precipitation around the tube for the 485°C sample after reorientation highlighting that the morphology and distribution of the hydrides across the tube remains quite constant.

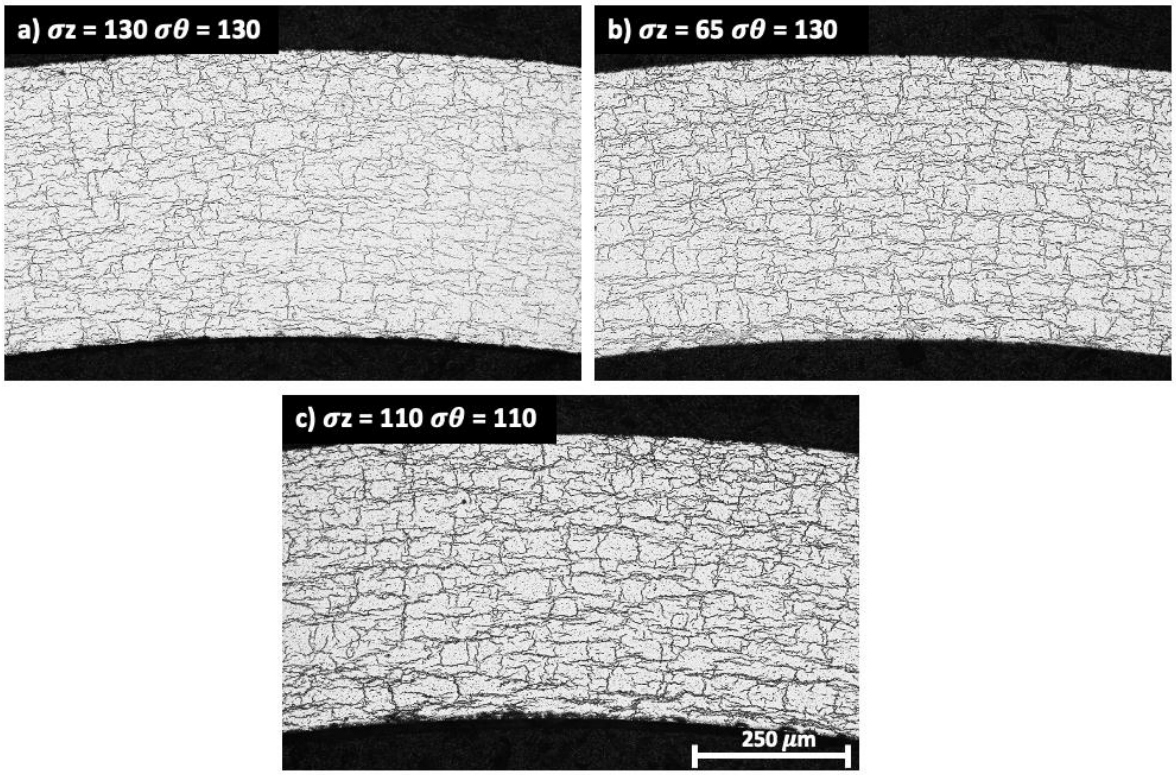

Figure 7.2 Evolution of the hydride precipitation at the three different stress conditions for the 520°C highlighting that the distribution and extent of radial hydride precipitation does not vary drastically for the three different stresses.

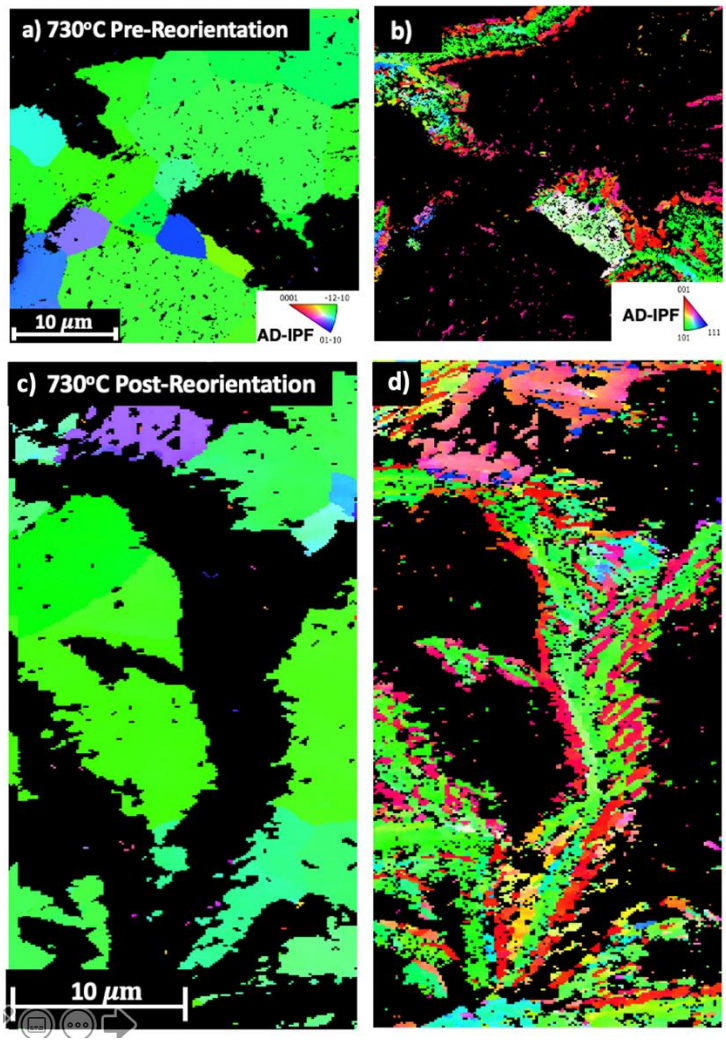

Figure 7.3 EBSD maps of the 730°C sample before and after reorientation

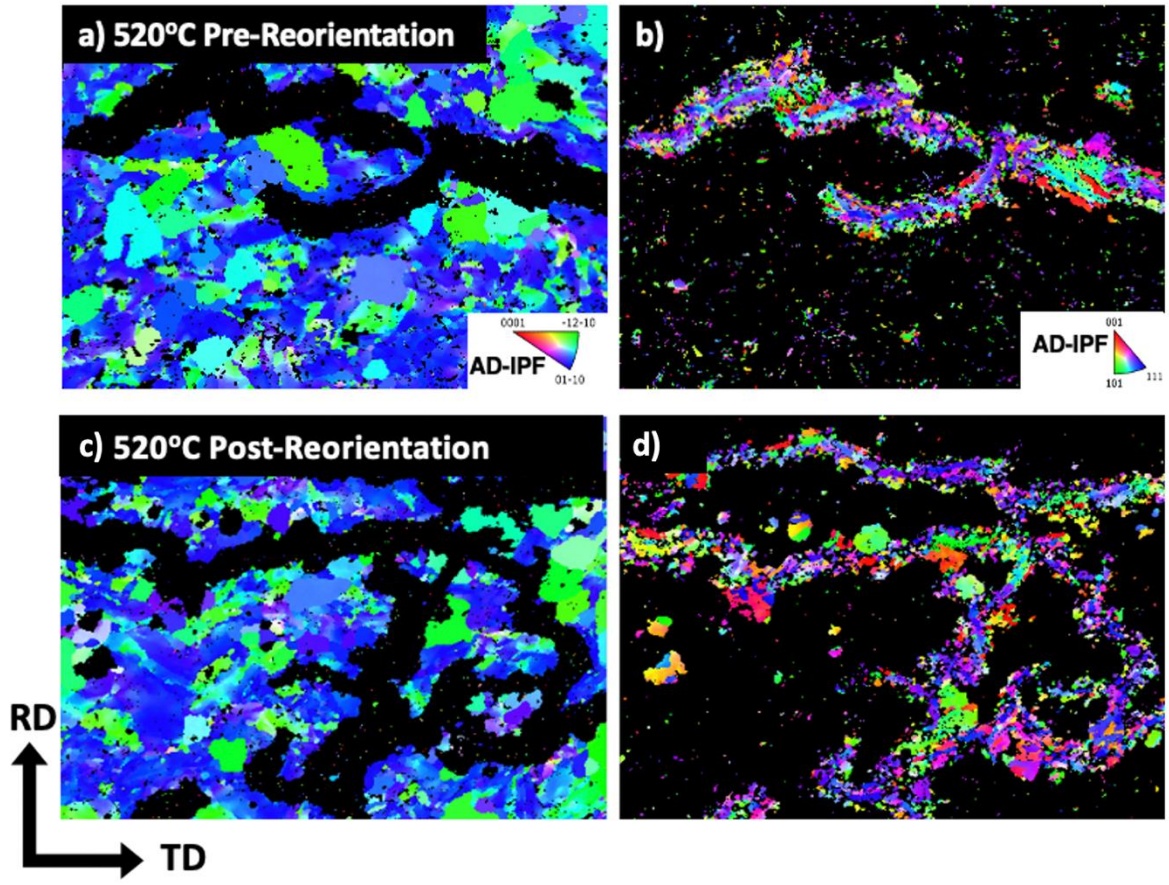

Figure 7.4 EBSD maps of the520°C sample before and after reorientation